Inversion of the Attenuated Radon Transform for Non-Parallel Geometries

Tianfang Li, Jiangsheng You, Junhai Wen, and Zhengrong Liang

***Abstract*—In this work, we first introduced a reorganized form of the Novikov's inversion formula for the attenuated Radon transform with parallel-beam geometry which utilizes the conventional filters (such as the Shepp-Logan, Hanning, etc.) to simplify image reconstruction procedures. Then we developed an accurate reconstruction method for non-parallel beam geometries. The method contains three major steps: (1) one-dimensional rebinning using phase-shifting technique, (2) performing non-uniform Hilbert transform, and (3) applying the reorganized Novikov's formula. Numerical evaluations demonstrated its computational efficiency and sound stability to different levels of Poisson noise. It also seemed to be very robust to different settings of fan-beam geometry from very long to very short focal lengths without affecting the reconstruction accuracy.**

I. Introduction

QANTIATIVE reconstruction for single photon emission computed tomography (SPECT) with compensation for non-uniform attenuation is mathematically formulated as a task of inverting the attenuated Radon transform (AtRT). A closed-form inversion formula for parallel-beam (PB) geometry was derived by Novikov using wave propagation theory in 2000 [1]. Thereafter, a generalized filtered backprojection (FBP) algorithm, which is based on a direct discretization of the Novikov's inversion formula, was developed to demonstrate the feasibility for quantitative SPECT imaging with PB collimation geometry [2, 3].

In the generalized FBP algorithm, the divergence operation (which also can be understood as a filtering process) has to be performed, in addition to the well-established filtering and backprojection steps. This differs from the classical FBP algorithm in which only one filtering step is needed. Also, numerical evaluations of the generalized FBP implementation turned out to be less stable than its classical FBP analogue [4, 5]. By manipulating the divergence operation, the Novikov's inversion formula can be reorganized into two parts each has an explicit meaning [6]. One part has a major contribution to the image reconstruction and has the classic FBP form. The other part is a correction component, which is insensitive to noise and also has the classic FBP form. This paper explores the potential of the reorganized formula to non-parallel beam (NPB) geometries, since in many clinical applications, NPB collimation geometries are desired, such as fan-beam (FB), asymmetrical fan-beam (AsF), and spatially varying focal length fan-beam (VFF) collimation geometries [7, 8, 9].

For FB geometry, an explicit inversion formula was discovered by Bukhgeim and Kazantsev [10, 11]. Their algorithm performs well when a specific equi-angular FB sampling is used [10]. However, applying their algorithm to other geometries, for example an equi-spatial FB sampling geometry, is not straightforward. The challenge becomes even severer for deriving an explicit inversion formula for other more complicated geometries, such as the AsF and VFF geometries mentioned above.

To the best of our knowledge, there is not yet a unified exact inversion formula for the AtRT under NPB geometries, except for the ray-driven technique we developed previously [12]. This technique is built on the fact that a single datum in the NPB measurements corresponds to a single datum in the PB dataset, representing one line integral. Due to the linearity of the inversion AtRT (which can be considered as a weighted summation or filtered backprojection operation), each line integral can be processed separately; therefore, the Novikov's inversion formula for the PB AtRT can be applied to perform the desired reconstruction in a NPB geometry ray-by-ray. However, the computational cost of this ray-driven technique is considerably high as known as $O(N^4)$, as compared to $O(N^3)$ of the Novikov's inversion formula for parallel geometry [2, 3].

In this work, we developed a new reconstruction algorithm for the inversion of the AtRT with NPB geometries, which preserves the same accuracy and efficiency as the original inversion procedure for PB geometry. This new algorithm is based on the reorganized Novikov's explicit inversion formula, phase shifting technique and non-uniform Hilbert transform (HT). Its derivation is presented for the VFF geometry, where the FB geometry is a special case. Numerical studies were performed for equi-spatial FB, VFF, and AsF geometries in the presence of strong non-uniform attenuation coefficient medium, similar to that occurs in the human thorax. Stability of the algorithm was tested with different focal length FB settings and with different levels of noise.

Manuscript received by October 20, 2004. This work was supported in part by the National Heart, Lung and Blood Institute under Grant HL54166.

T. Li, J. Wen, and Z. Liang are with the Department of Radiology, State University of New York (SUNY) at Stony Brook, NY 11794.

J. You was with SUNY at Stony Brook, NY 11794. He is now with Image Automation, Inc., Bedford, NH 11000.

II. NOVIKOV'S INVERSION FORMULA

Described below are the Novikov's original inversion formula and its two-component reorganization, in which the major component is in a classical FBP form.

A. Review of Novikov's Inversion Formula

Let $f(x,y)$ denote a function in space R^2, and $f_\theta(s,t) = f(s\cos\theta - t\sin\theta, s\sin\theta + t\cos\theta)$ be the same function in the Cartesian coordinate system (s,t) after rotation by an angle θ along the anti-clockwise direction. For simplicity, we introduce two vector symbols of $\vec{j} = (\cos\theta, \sin\theta)$ and $\vec{k} = (-\sin\theta, \cos\theta)$, and one complex symbol of $i = \sqrt{-1}$.

If $f(x,y)$ represents the distribution of radiotracer concentration inside the body in SPECT imaging. The γ photons, emitted from the radiotracer, are attenuated inside the body with coefficient distribution $\mu(x,y)$ before they arrive at the detector. Let $p(s,\theta)$ be the accumulated photon counts at position s along detector view angle θ in PB geometry, then

$$p(s,\theta) = \int_{-\infty}^{\infty} f_\theta(s,t)\exp[-a_\theta(s,t)]dt, \tag{1}$$

where $a_\theta(s,t) = \int_t^{\infty} \mu_\theta(s,\tau)d\tau$.

Using the conventions in [1], the Novikov's inversion formula for (1) can be expressed as follows

$$f(\vec{r}) = \frac{1}{4\pi}\mathbf{div}\int_0^{2\pi}\vec{j}[\exp([\mathbf{D}\mu]_\theta(s,t))\, g_\mu(s,\theta)]\Big|_{\substack{s=\vec{r}\bullet\vec{j}\\ t=\vec{r}\bullet\vec{k}}} d\theta \tag{2}$$

where

$$g_\mu(s,\theta) = \exp(-h_1)\cos(h_2)[\mathbf{H}\cos(h_2)\exp(h_1)[\mathbf{R}_\mu f]](s,\theta) + \exp(-h_1)\sin(h_2)[\mathbf{H}\sin(h_2)\exp(h_1)[\mathbf{R}_\mu f]](s,\theta) \tag{3}$$

with $h_1 = \tfrac{1}{2}[\mathbf{R}\mu](s,\theta)$ and $h_2 = [\mathbf{H}h_1](s,\theta)$. The mathematical operators in (2) and (3) are defined below

Hilbert transform: $$[\mathbf{H}g](s) = \frac{1}{\pi}\mathrm{pv}\int_{-\infty}^{\infty}\frac{g(\tau)}{s-\tau}d\tau \tag{4}$$

Half line integral: $$[\mathbf{D}\mu]_\theta(s,t) = \int_t^{\infty}\mu_\theta(s,\tau)d\tau \tag{5}$$

Radon transform: $$[\mathbf{R}f](s,\theta) = \int_{-\infty}^{\infty} f_\theta(s,t)dt \tag{6}$$

Attenuated Radon transform:

$$[\mathbf{R}_\mu f](s,\theta) = \int_{-\infty}^{\infty} f_\theta(s,t)\exp\{-[\mathbf{D}\mu]_\theta(s,t)\}dt \tag{7}$$

Detailed derivation of the Novikov's inversion formula can be found [1].

B. Classic FBP Version of Novikov's Inversion Formula

In [3], Natterer gave a very brief description on moving the divergence operator into the integral of equation (2), but the derivative was done by finite difference, which is similar to that of [2]. By moving the divergence operator and reorganizing the Novikov's inversion formula, we obtained a classical FBP version [6]. The detailed derivation is given below. First we introduce some utility definitions as follows.

Sign convolution:

$$[\tilde{\mathbf{D}}\mu]_\theta(s,t) = \int_{-\infty}^{\infty}\mu_\theta(s,t)\,\mathrm{sign}(\tau - t)d\tau \tag{8}$$

Complex combination:

$$\begin{aligned}[\tilde{\mathbf{C}}\mu]_\theta(s,t) &= \frac{1}{2}([\tilde{\mathbf{D}}\mu]_\theta(s,t) - i\,[\mathbf{HR}\mu](s,\theta)) \\ &= [\tilde{\mathbf{D}}\mu]_\theta(s,t) - \frac{1}{2}(\mathbf{I} + i\,\mathbf{H})[\mathbf{R}\mu](s,\theta))\end{aligned} \tag{9}$$

Differential and Hilbert transform:

$$[\mathbf{T}g](s) = \frac{1}{\pi}\mathrm{pv}\int_{-\infty}^{\infty}\frac{g'(\tau)}{s-\tau}d\tau \tag{10}$$

Weighted Radon transform:

$$[\tilde{\mathbf{R}}_\mu f](s,\theta) = \int_{-\infty}^{\infty} f_\theta(s,t)\exp\{-[\tilde{\mathbf{C}}\mu]_\theta(s,t)\}dt. \tag{11}$$

Using these definitions, the Novikov's inversion formula can be rewritten as

$$f(\vec{r}) = \mathrm{Re}\frac{1}{4\pi}\int_0^{2\pi}[(W_\theta(s,t)\mathbf{T} + W_\theta^1(s,t)\mathbf{H})\,\tilde{g}_\mu](s,\theta)]\Big|_{\substack{s=\vec{r}\bullet\vec{j}\\ t=\vec{r}\bullet\vec{k}}} d\theta \tag{12}$$

where $\tilde{g}_\mu(s,\theta) = [\tilde{\mathbf{R}}_\mu f](s,\theta)$, $W_\theta(s,t) = \exp\{[\tilde{\mathbf{C}}\mu]_\theta(s,t)\}$ (8) and $W_\theta^1(s,t) = \frac{\partial}{\partial s}W_\theta(s,t)$.

Now the inversion formula is expressed by two terms. It is easy to see that the first term $\int_0^{2\pi}[(W_\theta(s,t)\mathbf{T})\,\tilde{g}_\mu](s,\theta)]\Big|_{\substack{s=\vec{r}\bullet\vec{j}\\ t=\vec{r}\bullet\vec{k}}} d\theta$ is in the classic (weighted) FBP form, where the discretization of the operator $\mathbf{T}$ is understood as the traditional filtering process with the Ramp, Shepp-Logan, Hanning, or the like filters, and the weighting factor $W_\theta(s,t)$ depends only on the given attenuation map.

We also found that the first term in equation (12) dominates the reconstruction result, while the second term serves as only a minor correction. In the case of uniform attenuating medium, it can be proved that the second term contributes in the low frequency band $|\omega| < \frac{\mu}{2\pi}$ only. Since the differential operation usually amplifies the high-frequency components in numerical implementation, another advantage of formula (12) is that the divergence operation only exists in the second term (with minor contribution) of the reconstruction formula.

III. Reconstruction for NPB Geometries

In this section, we discuss how to apply the Novikov's inversion formula for NPB geometries. The VFF geometry is used for derivation of the reconstruction formula.

A. 1D Rebinning with Phase Shifting.

In Figure 1, a VFF geometry for SPECT is shown. Let $g(\beta,s)$ denote the projection data in the VFF geometry, and $p(\theta,l)$ be the projection data in the PB geometry. If a full scan is performed along a circular orbit for each geometry, then $g(.)$ and $p(.)$ are 2π periodic functions of the view angle β and θ, respectively, and are related, as shown in Figure 1, by the following equation

$$g(\beta,s)=p(\beta+\tan^{-1}[\frac{s}{F(s)}],\frac{s[F(s)-R]}{\sqrt{s^2+F^2(s)}}).$$

With Fourier transform, it is easy to show that

$$p(\varphi,\frac{s[F(s)-R]}{\sqrt{s^2+F^2(s)}})=\sum_n \widetilde{G}_n(s)\exp(in\varphi)$$

where

$$G_n(s)=\int_0^{2\pi} g(\beta,s)e^{-in\beta}d\beta,$$

therefore, re-phased parallel data p with non-uniform sampling along radial distance axis are achieved from the VFF data.

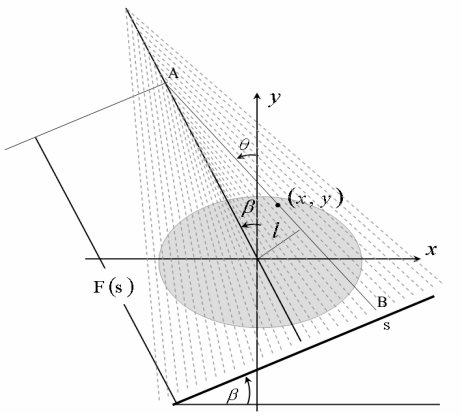

Figure 1: Two-dimensional presentation of a varying focal-length fan-beam geometry.

B. Non-Uniform HT

The explicit inversion formula (12) is exact for continually sampled data under PB geometry. By another 1D linear interpolation along the radial direction, addition to the phase shift above, it would be straightforward to apply the inversion for the image reconstruction. However, this usually results in the loss of reconstruction resolution [13], hence will not be explored in this work. In the following, we will retain the non-uniformly sampled projection data $p(\varphi,\xi)$ with $\xi=\frac{s[F(s)-R]}{\sqrt{s^2+F^2(s)}}$, and modify their related weighting functions in the inversion formula (12), then employ non-uniform HT to ensure an accurate image reconstruction.

Since for NPB geometries, it is often the case that s is evenly sampled, for example in $[-s_0,s_0]$, then ξ becomes non-evenly sampled. For any functional $g(\xi)$ that is sampled on non-uniform grids $\xi_i=\frac{s_i[F(s_i)-R]}{\sqrt{s_i^2+F^2(s_i)}}$, its discrete HT must be carefully evaluated. One method would be using the trapezoidal rule for a functional $g(\xi)$ as follows

$$[\mathbf{H}g](\xi_i)=\sum_{j\neq i}^{N} g(\xi_i)\frac{1}{\pi(\xi_j-\xi_i)}\Delta_j,\quad \Delta_i=\frac{1}{2}(\xi_{i+1}-\xi_{i-1}). \quad (13)$$

By our previous study [6], however, it is found that the direct implementation of HT via (13), which is essentially a convolution with $1/\pi x\ \ (0,\ if\ x=0)$, can result in the loss of image resolution. To avoid this possible drawback, we adopt the same form of a low-pass filter used by Natterer for the HT [3]:

$$[\mathrm{H}_\Omega g](\xi)=\int_{-\infty}^{\infty}\frac{1-\cos(\Omega(\xi-t))}{\pi(\xi-t)}g(t)dt\ , \quad (14)$$

where $\Omega>0$ is the bandwidth. Then the HT of a functional $g(\cdot)$ sampled on the non-uniform grid $\xi(s)$ can be derived as

$$[\mathbf{H}_\Omega g](\xi_0)=\int_{-\infty}^{\infty}\frac{1-\cos(\Omega(\xi_0-\xi(s)))}{\pi(\xi_0-\xi(s))}g(\xi(s))J(s)ds$$

$$J(s)=\left[sF'(s)\left(s^2+RF(s)\right)+\left(F(s)-R\right)F^2(s)\right]/\left(s^2+F^2(s)\right)^{3/2}ds. \quad (15)$$

C. Reconstruction Procedure

We summarize the implementation of the proposed reconstruction algorithm as follows:

1) Modify the non-parallel projection data $g(\beta,s)$ to obtain the re-phased data $p(\varphi,\xi)$ by the use of the phase shifting technique: $p(\varphi,\xi)=\sum_n \exp[-in\tan^{-1}(\frac{s}{F(s)})]G_n(s)\exp(in\varphi)$, and $\xi=\frac{s[F(s)-R]}{\sqrt{s^2+F^2(s)}}$;

2) Calculate $W_\theta(s,t)$ and $W_\theta^1(s,t)$, using $h_1(\varphi,\xi)=\frac{1}{2}[\mathbf{R}\mu]_\varphi(\xi)$, $h_2=[\mathbf{H}h_1](\varphi,\xi)$, and $[\widetilde{\mathbf{D}}\mu]_\varphi(\xi,t)=[\mathbf{D}\mu]_\varphi(\xi,t)-h_1(\varphi,\xi)$, where the non-uniform HT of equation (15) is needed;

3) Apply equation (12) for reconstruction.

The above derivation is based on the VFF geometry, but it is straightforward to apply the reconstruction formula to other NPB geometries by selecting different focal length functions $F(s)$. It is easy to see that the complexity of the implementation for NPB geometry reconstruction is in the same order as that for the PB case. Numerical studies on the

computational efficiency and accuracy, as well as several other properties, are presented in the next section.

IV. Simulation Results

In this section, we present computer simulation studies on the proposed NPB geometry reconstruction algorithm. First, we test the algorithm for typical FB, VFF, and AsF geometries. Secondly, we study the stability of the algorithm to the variation of the FB focal length. Finally, the robustness to the data noise is investigated for the VFF geometry. The reconstruction time is also reported.

The emission map used in the simulations is the 2D Shepp-Logan mathematic phantom. The attenuation map contains several ellipse structures with three different attenuation coefficient values similar to those of water, soft tissues, and bones in human being, see Figure 2. Emission map $f(x, y)$ and attenuation map $\mu(x, y)$ were sampled in a grid of 256×256. Projections $[\mathbf{R}_\mu f](s, \theta)$ were sampled with 256 bins by 256 views evenly spaced on 360 degrees for a corresponding geometry. Each projection datum was computed by the line integral through the phantom maps. Without specifically stating, the same configurations will be applied in the following simulations.

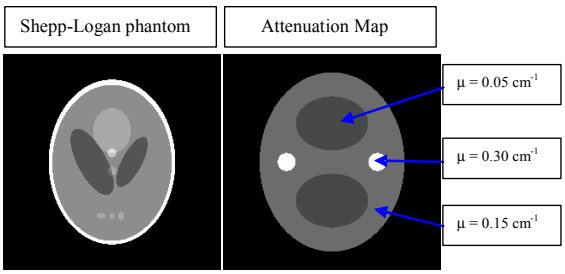

Figure 2: Two-dimensional presentation of the emission phantom (left) and the attenuation map (right).

A. Image Reconstruction for FB, VFF, and AsF Geometries

For FB geometry, the focal length is 62.5 cm, the radius of rotation (ROR) is 17.5 cm, the detector size/length is 48 cm (evenly sampled by 256 detector bins of size 0.19 cm), and the image pixel size is 0.125 cm. For the VFF geometry, the focal length function is $F(s) = as^2 + b$ with $a = 0.24$, and $b = 40$. The detector size/length remains 48 cm (evenly sampled by 256 detector bins of size 0.19 cm), and the ROR also remains 17.5 cm. The focal length varies from minimum of 40 cm to maximum of 178.24 cm (when s = 24 cm). For the AsF geometry, its configuration is presented in Figure 3. The simulated projections and their reconstructed results are presented in Figure 4.

From the above three experiments, the proposed reconstruction algorithm demonstrated good performance for all FB, VFF, and AsF geometries. The computation time for each one is 49 second, 53 second, and 52 second, respectively, on a PC Pentium III with 550 Mhz CPU and 256 MB RAM. The computation time for the PB geometry with the original Novikov's formula is 45 second on the same machine.

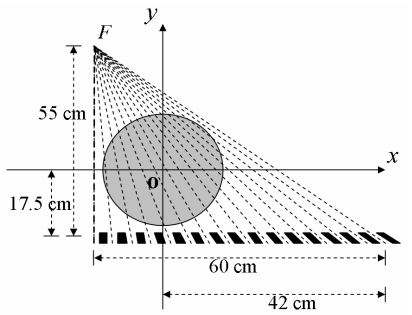

Figure 3: Asymmetrical fan-beam geometry.

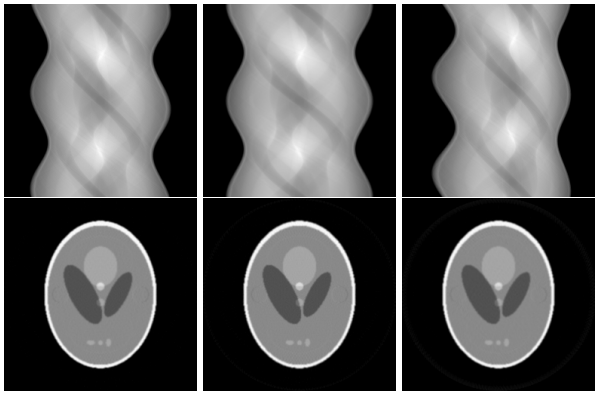

Figure 4: The simulated sinograms (top row) and their reconstructed images (bottom row) for FB, VFF, and ASF geometry (from left to right), respectively.

B. Stability to the Variation of the Focal Length

In this section, another property of the proposed reconstruction algorithm – the stability to the variation of the focal length is presented, which reflects the system amplification factor. For this study, the simulations were performed for the FB geometry, with the focal length varying from very large (infinity) to very short one. The detector size/length is 48 cm, and the ROR remains 17.5 cm.

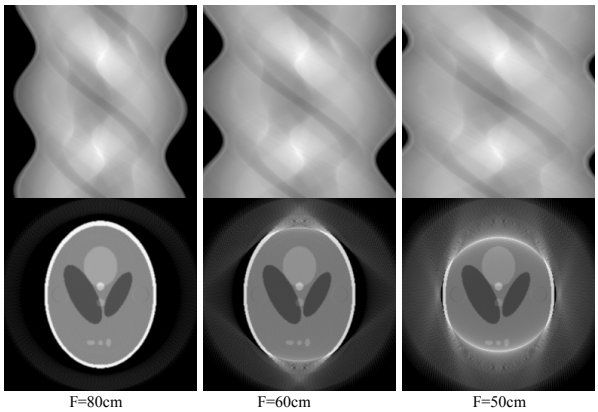

Figure 5: The simulated sinograms (top) and their reconstruction results (bottom) for the fan-beam geometry of different focal lengths.

The simulated sinograms and corresponding reconstructed images are shown in Figure 5. As the focal length becomes

shorter, the reconstructed images remain the same quality. The reconstruction generates artifact-free images within the central FOV region, even if truncation occurs at the FOV periphery (for example, when the focal length reduces to 60 cm and 50 cm in Figure 5). These results demonstrated the stability of the proposed algorithm to the focal length variation.

C. Robustness to the Noise in Measurements

To include noise in simulation studies, each datum in the simulated noise-free VFF projections (in section ***A***) above was assumed as the mean or average from its multiple measurements. This mean was inputted to a Poisson random-number generator to provide a noisy realization of the datum. Three different noise-level sinograms were generated by scaling the noise-free data and then adding Poisson noise. The count levels are approximately, for each view of 256 bins, (1) 1,000,000 counts, (2) 100,000 counts, and (3) 10,000 counts. The noisy reconstructed images are shown in Figure 6.

Apparently, some details in the reconstructed images disappear due to the Poisson noise. Also, the reconstructed image includes randomized spots across the FOV that are common to FBP or other analytical and iterative reconstructions of Poisson-noise projections without regularization or penalty on the noisy data. However, a fairly good compensation for non-uniform attenuation is still observed in these noisy cases. In addition, no obvious artifact is seen with the increase of the noise. Accurate treatment of the Poisson noise or extraction of signal from the Poisson noise sinogram for the inversion formula or reconstruction algorithm is an important issue, and detailed discussion is beyond the scope of this work [14].

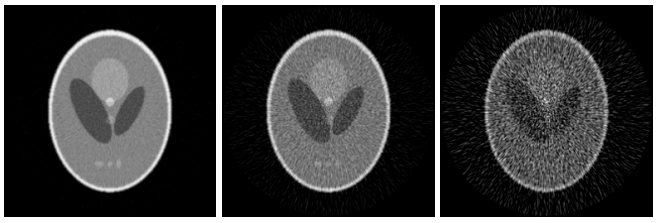

(a) (b) (c)

Figure 6: The simulated sinograms with different levels of noise (top) and their corresponding reconstructed images (bottom) under the VFF geometry. (a) 1M counts per view of 256 bins, (b) 100K counts per view of 256 bins, and (c) 10K counts per view f 256 bins.

V. Conclusions

In this work, we presented a two-term representation of the Novikov's inversion formula, and developed an algorithm for image reconstruction with NPB geometries. The algorithm re-aligns the non-parallel projection data along the view direction for all detector bins by the phase-shifting technique and implements appropriately the non-uniform HT, so that the reorganized Novikov's inversion formula can be extended accurately and efficiently from parallel to non-parallel geometries. By numerical simulations we showed that the presented NPB algorithm has comparable reconstruction quality and computation efficiency as the PB geometry formula and is robust to the variation of focal length (which is related to the system amplification factor) and the quantum noise in measurements. The inversion procedure discussed in this paper provides a mathematically sound and unique solution to the attenuation problem, which is not only of theoretical interest, but also has practical significance in the sense that it may lead to quantitative SPECT in the future with additional compensation for other degradation factors, such as PSF (point spread function) variation, scatter, and the Poisson noise [15-18].

VI. References

[1] R. G. Novikov, "An inversion formula for the attenuated X-ray transformation", Preprint, May of 2000, and in *Ark. Math*., vol. 40, pp. 145-167, 2002.

[2] L. A. Kunyansky, "A new SPECT reconstruction algorithm based on the Novikov explicit inversion formula", *Inverse Problems*, vol. 17. pp. 293-306, 2001.

[3] F. Natterer, "Inversion of the attenuated Radon transform", *Inverse Problems*, vol. 17. pp. 113-119, 2001.

[4] J-P Guillement, F. Jauberteau, F. Kunyansky, R. Novikov and R. Trebossen, "On single-photon emission computed tomography imaging based on an exact formula for the nonuniform attenuation correction", *Inverse Problems*, vol. 18. pp. L11-9, 2002.

[5] J-P Guillement and R. Novikov, "A noise property analysis of single-photon emission computed tomography data", *Inverse Problems*, vol. 20. pp. 175-198, 2004.

[6] J. You, T. Li, J. Wen, and Z. Liang, "A classic FBP implementation of Novikov's inversion of attenuated Radon transform for quantitative SPECT imaging", Preprint, 2004.

[7] R. J. Jaszczak, J. Li, H. Wang, and R. E. Coleman, "SPECT collimation having spatially variant focusing (SVF)," *J. Nucl. Medicine*, vol. 33(5), pp. 891, 1992.

[8] G. L. Zeng, G. T. Gullberg, R. J. Jaszczak and J. Li, "Fan-beam reconstruction algorithm for a spatially varying focal length collimator," *IEEE Trans. Med. Imaging*, vol. 12, pp. 575-582, 1993.

[9] W. Chang, S. Loncaric, G. Huang and P. Sanpitak, "Asymmetrical fan beam transmission CT on SPECT system," *Phys. Med. Biol*., vol. 40, pp. 913-928, 1995.

[10] A. A. Bukhgeim, S. G. Kazantsev, "Inversion formula for the fan-beam attenuated Radon transform in a "unit disk", Preprint, 2002.

[11] E. V. Arbuzov, A. L. Bukhgeim, and S. G. Kazantsev, "Two-dimensional tomography problems and the theory of A-analytic functions", *Siberian Advances in Mathematics*, vol. 8, pp. 1-20, 1998.

[12] J. Wen, T. Li and Z. Liang, "An analytical inversion of non-uniformly attenuated Radon transform with variable focal-length fan-beam collimators", *IEEE Trans. Nucl. Science*, vol. 50, pp. 1541-1549, 2003.

[13] X. Pan and L. Yu, "Image reconstruction with shift-variant filtration and its implication for noise and resolution properties in fan-beam computed tomography," *Medical Physics*, vol. 30(4), pp. 590-600, 2003.

[14] J. Cheng, Z. Liang, J. Ye, C. Cabahug, Z. Oster, and D. Harrington "Accurate treatment of Poisson noise for quantitative reconstruction of brain SPECT," J. Nucl. Medicine, vol. 37: pp. 218, 1996.

[15] T. Li, J. Wen, and Z. Liang, "Analytical compensation for spatially variant detector response in SPECT with varying focal-Length fan-beam collimators", *IEEE Trans. Nucl. Science*, vol. 50, pp. 398-404, 2003.

[16] X. Li, G. Han, H. Lu, L. Li, T. Li, and Z. Liang, "A new scatter estimation method using triple window acquisition to fit energy spectrum," *J. Nucl. Medicine*, vol. 42, pp. 194, 2001.

[17] T. Li, X. Li, J. Wang, J. Wen, H. Lu, J. Hsieh, and Z. Liang, "Nonlinear sinogram smoothing for low-dose X-ray CT," *IEEE Trans. Nucl. Science*, in press, 2004.

[18] T. Li, J. Wen, G. Han, H. Lu, and Z. Liang, "Evaluation of an efficient compensation method for quantitative fan-beam brain SPECT reconstruction," *IEEE Trans. Med. Imaging*, in press, 2004.